The FASEB Journal

FASEB
Federation of American Societies for Experimental Biology

RESEARCH ARTICLE OPEN ACCESS

ELV-N34, RvD6-Isomer, or NPD1 Halt Replication of SARS-CoV-2 Omicron BA.5 Virus in Human Lung and Nasal Cells

Jorgelina M. Calandria[1] | Haydee E. P. Bazan[1] | Surjyadipta Bhattacharjee[1] | Marie-Audrey I. Kautzmann[1] | Nicholas J. Maness[2] | Nicolas G. Bazan[1]

[1]Neuroscience Center of Excellence, Louisiana State University Health New Orleans, New Orleans, Louisiana, USA | [2]Tulane National Primate Research Center, Covington, Louisiana, USA

Correspondence: Jorgelina M. Calandria (jcalan@lsuhsc.edu) | Haydee E. P. Bazan (hbazan1@lsuhsc.edu)

Received: 11 December 2024 | **Revised:** 1 April 2025 | **Accepted:** 14 April 2025

Funding: This work was supported by EENT Foundation of New Orleans.

Keywords: autophagy | COVID-19 | omega-3 fatty acids

ABSTRACT

Current vaccines rely on the sequence of Spike (S) protein to induce immunity against the severe acute respiratory coronavirus-2 (SARS-CoV-2) virus. Because of the high mutation rate of the viral S protein, new mutant strains are developed to generate new infectivity profiles. Bioactive lipid mediators (LMs) derived from docosahexaenoic acid (DHA) are synthesized on demand to sustain homeostasis. The purpose of this study was to determine the action of selected LMs in the viral replication of SARS-CoV-2 Omicron BA.5 variant in human lung and nasal epithelial cells. Cells from healthy donors were infected with Omicron BA.5 for one hour and treated with 500 nM Elovanoid (ELV)-N32, ELV-N34, Resolvin D6 isomer (RvD6i), Neuroprotection D1 (NPD1), or vehicle before and after infection. Impedance was recorded to determine cell death by infectivity. Cells were then immunostained for nucleocapsid (N) protein, microtubule-associated protein 1B-light chain 3 (LC3B), and autophagic proteins. N and S RNA were measured to assess the synthesis of viral components. The addition of ELV-N34 or RvD6i decreased the synthesis of N RNA by 76.7% and 96.9%, respectively, in lung primary culture, while NPD1 exerted the same effect in nasal epithelial cells (61.7% reduction). In lung cells, transcription of autophagy-related gene-3 (ATG3) and Sequestosome 1 (SQSTM1/p62), components of the autophagy initiation process, decreased compared to the non-treated infected cells. The results suggest that specific LMs prevent viral autophagy machinery hijacking, leading to a decrease in BA.5 replication. This novel effect of the bioactive LMs as antivirals, regardless of the protein sequence, would potentially complement vaccination and other prevention and treatment therapeutics.

1 | Introduction

The complex evolution of the severe acute respiratory coronavirus-2 (SARS-CoV-2) since its inception has been well documented [1]. The fast change in the sequences has allowed the virus to bypass the adaptive immune response even when this immunity was modulated by the immunization practices [2, 3]. Antiviral strategies that target specific proteins, like S or M viral proteins or activities of viral components such as proteases NSP3 and NSP5 or other functions required for the viral cycle, have been investigated [4]. However, the restoration of normal cell functions disrupted by the viral infection was not a goal of these approaches.

Autophagy is a complex pathway that eukaryotic cells use to eliminate debris (e.g., senescent organelles and old proteins) and

maintain homeostasis. Several studies have shown that SARS-CoV-2 hijacks cellular elements involved in autophagy to use them for its replication [5–9]. The virus selectively modulates proteins involved in the formation of the phagophore to promote a double-membrane vesicle (DMV) structure that will contain viral RNA synthesis dedicated to the replication of SARS-CoV-2 [10]. Therefore, restoring normal cellular function will help the cell stop the viral cycle, decrease the efficiency of replication, and resume the antigen presentation process to allow the immune system to respond, thus avoiding the spread to other cells.

Elovanoids (ELVs) are bioactive lipids synthesized from very long fatty acids (VLFA) that are derived from omega-3 fatty acid docosahexaenoic acid (DHA) [11]. The elongation of the DHA is performed by the enzyme ELOVL4 (elongation of very long chain fatty acids-4) and consists of a saturated extension of the carbon chain [12]. Previous studies have shown that ELVs reduce Wuhan strain SARS-CoV-2 entry into human alveolar cells in vitro via regulation of canonical mediators and protective signaling [13]. Moreover, ELVs act as anti-inflammatory agents in nasal epithelial cells [14], which are targets of SARS-CoV-2, as well as in lung alveolar cells. Furthermore, ELVs decrease autophagy in murine retinal epithelial cells "in vivo" [15] and nasal epithelial cells "in vitro" exposed to allergen [14]. In addition, another LM derived from DHA, Resolvin D6 isomer (RvD6i), is an anti-inflammatory found in tears that sustains corneal [16] and trigeminal nerve regeneration [16, 17] and decreases the expression of the ACE2 receptor of SARS-CoV-2 [18].

Here, we tested a group of bioactive lipids, including ELV-N32 and ELV-N34, Neuroprotectin D1 (NPD1), and RvD6i for their potential involvement in the modulation of autophagy and the viral cycle to explore the hypothesis that restoring homeostasis in infected cells will decrease the efficiency of viral replication, and that LMs could be used as an antiviral strategy to supplement current therapeutic treatments.

2 | Materials and Methods

2.1 | Impedance in Primary Cultures of Human Nasal and Alveolar Cells

Primary cell cultures of human alveoli and nasal epithelium derived from two healthy male donors, 72 years old for lung and 50 years old for nasal cell cultures, were used. Due to reported sex differences in the immune response in COVID-19–infected patients, with more severe outcomes among men [19] we only used male donor cells for these studies. Alveoli cells consisted of a mixed culture of ciliated cells, club cells, type I pneumocytes, and type II pneumocytes (PromoCell, HSAEpC) [13]. Fifteen thousand cells were incubated to confluency and maintained in the proprietary medium provided by Promocell with the addition of Pen/Strep 1X. Vero E6 cells (from ATCC CRL-1586) were cultured as described elsewhere [20]. The stocks of SARS-CoV-2 (SARS-CoV-2; 2019-nCoV/USA-WA1/2020 BEI# NR-52281) and Omicron subvariant BA.5 (Variant B.1.1.529.5) were generated in VeroE6 cells as previously described [20].

Nasal epithelial primary cell cultures were composed exclusively of epithelial cells due to the difficulties other types of nasal cells have in maintaining adherence in submerged monolayers. Cells were treated following the protocol schematized in Figures 1A and 2A. Briefly, lung and nasal cells plated in 96 well plates and 8 well chambers, respectively, were incubated with 500 nM of ELV-N32, ELV-N34, NPD1, or RVD6i for 24 h before being exposed to the virus. The infection was done by NJM in a BSL3 facility at Tulane National Primate Research Center. The BA.5 strain of SARS-CoV-2 was administered at Tissue Culture Infections Dose, 50% endpoint (TCID50) equal to 10 000 for one hour and removed. Fresh medium containing 500 nM of LMs or vehicle was re-applied, and the cells were incubated for 90 h. Before bringing the cells to the laboratory, they were inactivated by replacing the media with 2% paraformaldehyde (PFA) overnight at room temperature. To test the action of LMs in another virus strain, lung cells were infected also with the SARS-CoV-2 Wuhan strain at the same concentration that Omicron BA.5 was. To measure the effects of the lipids on SARS-CoV-2 infection, we used real-time cell analysis (RTCA) to determine impedance with the Agilent eSight system. The plates were loaded on the eSight instrument. Impedance was measured every 15 min, and an image was taken every hour for 90 h. Data was analyzed using Agilent RTCA Pro software.

2.2 | Immunocytochemistry

Immunostaining was performed as previously described [13]. Briefly, after fixation, permeabilization, and blocking, cells were incubated overnight at 4°C with the primary antibodies described in Table S1. DAPI (Thermo Fisher cat# D1306) was used for nuclear staining, and CellMask (Thermo Fisher cat# C10046) was used for cell membrane staining. Slides were mounted, and *Z*-stacks were obtained for 5 random fields in a FluoView 3000 laser confocal microscope. Images were processed with IMARIS 9.9 using the Cell module.

2.3 | Measurement of Gene Expression Real-Time PCR Using BioMark

After treatment, cells were homogenized using TRIzol reagent (Cat. #15596026L, Invitrogen, Thermo Fisher Scientific Inc., Waltham, MA, USA) according to the manufacturer's protocol. Total RNA was prepared using RNeasy columns (Cat. #74004, Qiagen, Valencia, CA, USA). RNA quantity and purity were assessed using the NanoDrop One spectrophotometer (Thermo Scientific). Reverse Transcription was performed with 10–100 ng of total RNA using the iScript cDNA Synthesis Kit (Bio-Rad, Hercules, CA, USA). HT-qPCR was performed as described in Reid et al. [21]. Briefly, 5 μL of qPCR reaction mixture contained 2.25 μL of diluted pre-amplified cDNA, 0.25 μL of DNA Binding Dye (Fluidigm), and 2.5 μL SsoFast EvaGreen Supermix with low ROX (Bio-Rad). The primer reaction mixture had a final volume of 5 μL and contained 2.5 μL Assay Loading Reagent (Fluidigm, South San Francisco, CA, USA) and 0.25 μL of a mix of all reverse and forward primers (Table S2), corresponding to a final concentration of 0.5 μM in the reaction. The BioMark 96.96 IFC (Integrated Fluidic Circuit) was first primed with an oil solution in the Juno Controller (Fluidigm) to fill the fluidic circuit. RT-qPCR Data Analysis: Raw data were pre-processed with the Real-Time PCR analysis software v4.1.3 (Fluidigm);

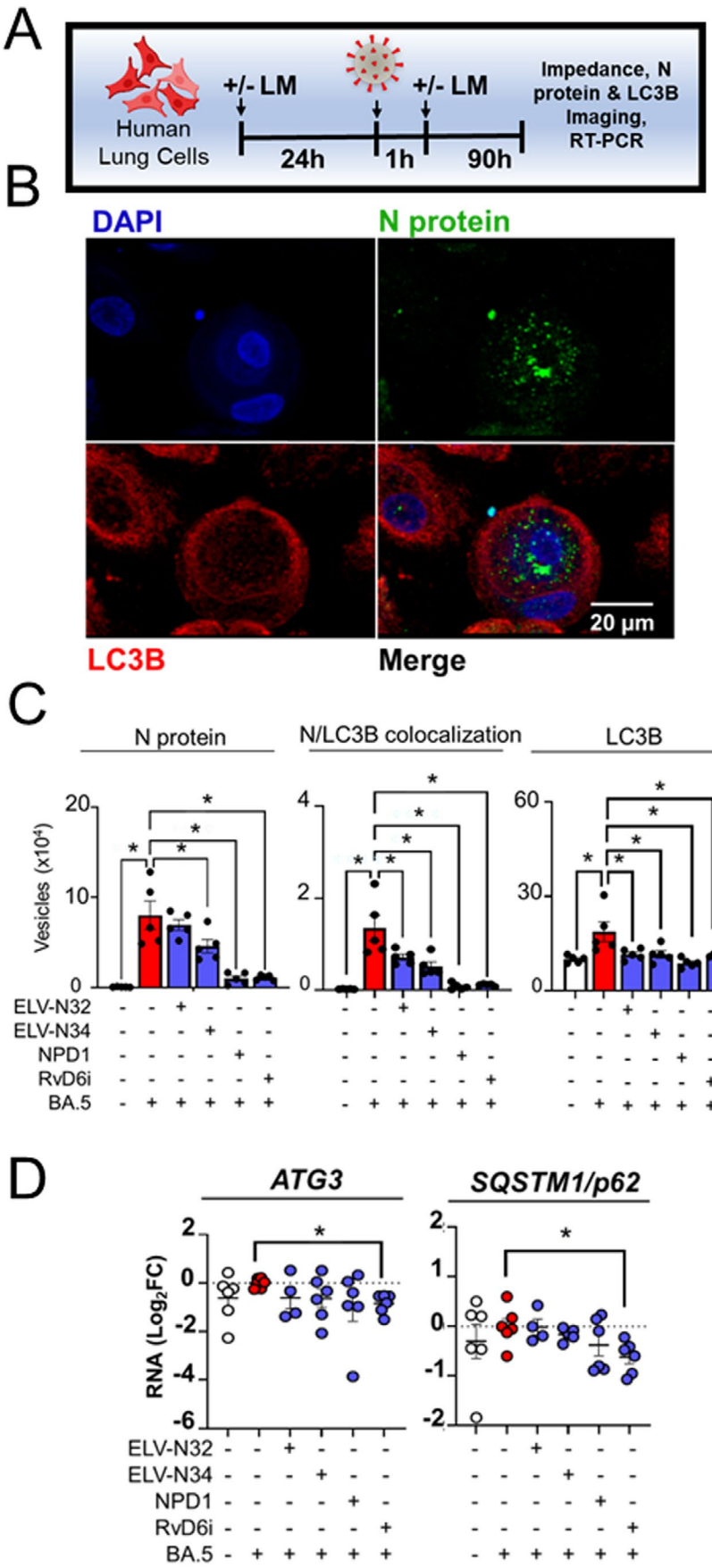

FIGURE 1 | Legend on next page.

FIGURE 1 | Bioactive lipid mediators reduced the vesicles containing Omicron N protein in lung cells but only RvD6i modulated expression of lipidation genes. (A) Schematic representation of the protocol used to infect lung cells. Human lung cells were incubated with 500 nM of ELV-N32, ELV-N34, NPD1, RvD6i or vehicle for 24 h, exposed to omicron BA.5 for one hour and then the impedance was recorded for 90 h in the presence or absence of vehicle or LM (Figure S1). After this period, the cells were fixed, immunostained, and analyzed using Imaris software. (B) Representative high magnification image of an infected lung cell depicting N virus protein, LC3B, a component of the LC3II lipidation complex that participates in the formation of vesicles in autophagy and phagocytosis (green and red, respectively), located in the proximity of the nucleus stained with DAPI (blue). (C) Quantification of vesicles containing N protein (left panel), LC3B (right panel), and N plus LC3B (middle panel) using Imaris Cell module of human lung primary cells treated as detailed in A. (D) Expression of ATG3 and SQSTM1/p62 messenger RNA via RT-PCR in lung cells infected with BA.5 in the presence or absence of LM. Five replicated samples were analyzed in each case. ANOVA and Tukey's honest significant difference test of the mean were used to determine statistical significance. $*p < 0.05$.

unspecific values were deleted based on melting-curve analysis. The relative mRNA expression levels of genes were calculated using the ΔΔCT method, following normalization to the geometric mean of housekeeping genes: PGK1, RPL13A, and TFRC, and calculation of fold of expression and transformation to logarithmic scale. This method amplifies both genomic and subgenomic RNA, but cannot discriminate between both RNAs.

2.4 | Real-Time Imaging of Lung Cells Migration and Replication

Ten thousand human lung cells passage 2 were plated per well in an Incucyte Imagelock 96-well Microplate (Sartorius cat# BA-04856; Sartorius Corp., Bohemia, NY) and incubated until 98% confluency. A scratch was made with a pipet tip following the fiduciary lines in all the wells. Four wells were assigned for each condition: Control, Vehicle (ethanol), and 500 nM ELV-N34, NPD1, and RvD6i. Similar to the impedance test, it was performed using eSight. The confluency was recorded for 90 h inside and outside the scratch (Figure S4C). The results of 3 pictures per well at a given time were analyzed and plotted using GraphPad software (GraphPad Software LLC; Boston, MA) to determine cell replication and migration.

2.5 | Statistical Analysis

Plots and statistical treatment were performed using GraphPad 10.0. The data were first analyzed using one-way analysis of variance (ANOVA) and multiple comparisons via Tukey's honest significant differences test. The pairwise comparison was performed using a two-tailed Student's *t*-test.

3 | Results

3.1 | RvD6i and ELV-N34 Reduce Infection of Omicron BA.5 in Human Lung Cells

Beta-coronaviruses can manipulate the host's autophagic components to replicate, assemble, and exit from the cells and, in doing so, avoid the anti-viral response of the organism [22–28]. Our previous studies showed that ELV-N34 decreases the entry of the Wuhan strain of SARS-CoV-2 into human lung cells in culture [13]. To investigate the effects of LMs in the replication and internal processing of SARS-CoV-2, we infected human lung and nasal cells with the Omicron BA.5 variant in the presence or absence of the bioactive LMs NPD1, ELV-N32, ELV-N34, or RVD6i as explained in Figures 1A and 2A. On confluent cultures, we measured the detachment of the cells due to virus infection using impedance-based xCELLigence technology. The biosensors monitor cell metrics, such as proliferation and adhesion strength, two properties proportional to the increase in the current resistance. The cell index of lung monolayers obtained from healthy male donors exposed to the MOI = 10 000 of the virus was plotted versus time (Figure S1B). Human lung cells display a triphasic curve that was broken down into three zones: an early phase of growth (fast growth), spanning from 5.3 to 14.3 h post-infection, a second growth (from 24.3 to 52.5 h) in which the slopes decreased, and a third phase of decay (from 69.3 to 89 h) where the cell detachment caused by the infection is more prominent (Figure S1B–E). During the first growth phase, the slopes of BA.5 alone or plus ELVs were similar (Figure S1C; Table S3). NPD1 addition increased the slope, while RvD6i treatment shows a slope below the non-treated infected cells. However, during the second phase, all the mediators surpassed the slope of growth recorded by the control and non-treated cells (Figure S1D; Table S3). During this phase, the assembly of the virions probably starts. The decay was also less pronounced when the cells were exposed to ELV-N34, NPD1, and RVD6i, suggesting a halt in the replication and exit of the viral particles from the cells (Figure S1E; Table S3). A cell line derived from green monkey kidney, Vero cells, infected with the original Wuhan strain of SARS-CoV-2 depicted similar trends when treated with the LMs (Figure S2); however, in this case, ELV-N32 was able to counteract the effects of the decrease in impedance to a greater extent than the rest of the LMs. We performed a scratch assay, without viral infection, for migration and replication of the lung cells using the same conditions as in the eSight assay to determine if that could influence the impedance changes observed (Figures S1 and S2). We observed a 2-to 4-fold increase in the replication of the cells in the first three hours (Figure S3) while there was no visible migration in all the LMs treatments (Figure S3C), picture with RvD6i treatment), suggesting that the changes in the impedance observed were not due to changes in the cell number or migration.

To determine the mechanisms involved in the life cycle of the virus that were perturbed by the LMs, we performed immunostaining targeting nucleocapsid viral protein (N) and Microtubule-associated proteins 1A/1B-light chain 3 (MAP1-LC3 or LC3B), a component of the autophagic machinery involved in the viral replication mechanism. The virus develops a double-membrane vesicle structure (DMV) that is produced by fragmentation of the Golgi system of the host cell

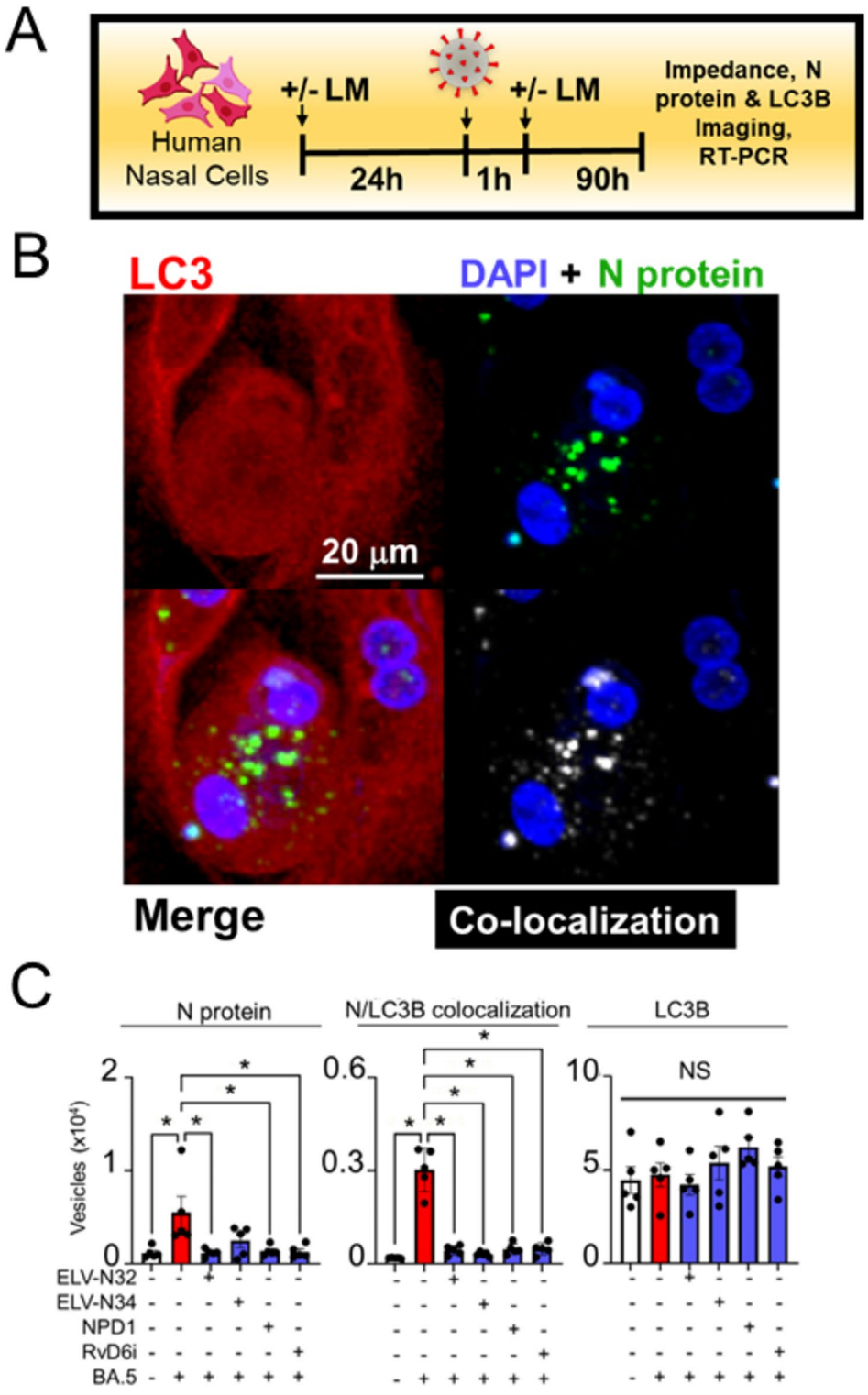

FIGURE 2 | Lipid mediators counteract the increase in Omicron N protein in nasal cells. (A) Schematic representation of the protocol used to infect nasal epithelial cells. Human nasal epithelial cells were incubated with 500 nM of LMs for 24 h and exposed to Omicron BA.5, and their impedance was recorded in the presence or absence of the LMs. (B) Representative image of infected nasal. N virus protein and LC3B were immunostained and analyzed for colocalization along the treatments (N protein = green; LC3B = red and nuclei = Blue; Colocalization in white). (C) Quantification of the colocalized N and LC3B using Imaris 10.0 cell module. ANOVA and Tukey's honest significant difference test of the mean were used to determine statistical significance. $*p < 0.05$.

[10] with the help of the host's LC3 [22, 24–27]. The process requires the action of conserved autophagy-related genes (Atg) that encode a number of ATG proteins. In lung cells, a fifth of the nucleocapsid signal colocalized with LC3B (Figure 1B,C), suggesting the involvement of the autophagy protein in one of the steps of the viral assembly/replication. Lung cells exposed

to BA.5 in the presence or absence of ELV-N32 and N34, NPD1, or RvD6i (Figure 1A) were used to measure the expression of transcripts encoding proteins involved in autophagy. Only RvD6i decreased the expression of two components of the lipidation of the phagophore that are involved in the expansion and completion of DMV formation: ATG3 and SQSTM1/p62 (Figure 1D). In addition, lung cells infected with the Wuhan strain, using the same protocol, show a similar decrease in N protein with ELV-34 and RvD6i, suggesting a virus strain-independent effect (Figure S4).

Altogether, these data suggest that in lung cells treated with ELV-N34, NPD1, and RvD6i, there is a decrease in the total content of N, that the LMs equally blocked the viral-driven LC3B increase, and that RvD6i reduced the expression of other autophagy players (ATG3 and SQSTM1/p62) involved in the formation of membranes of the autophagic machinery.

The results also demonstrate that there is a similar mechanism of action of the LMs regarding the type of strain or mutation, which suggests that the lipids are interfering with a fundamental mechanism that the virus uses for its infection.

3.2 | Nasal Epithelial Cells Showed a Different Behavior Than the Lung Cells in Their Response to BA.5 Infection and Lipid Mediators

Nasal epithelial primary cells from a male normal donor displayed only one phase of growth during the 90-h recording (Figure S5). Compared to human lung cells, this initial phase was longer and did not reach the plateau or the decay phases during the period in which the lung cells did. The linear part of the curve was analyzed using simple regression (Figure S5C). The slopes were steeper than the control and infected cells when treated with NPD1, ELV, and RVD6i (Table S5). To investigate the differences in the infection mechanism of SARS-Cov2 Omicron BA.5 between nasal and lung cells, the nasal cells were exposed to the virus following the same protocol (Figure 2A). N protein and LC3B were co-immunostained (Figure 2B) and analyzed for colocalization. Nucleocapsid protein was significantly reduced in cells treated with ELV-N32, NPD1, and RvD6i (Figure 2C, left panel). LC3B was not affected by the viral infection or the addition of the LM (Figure 2C, right panel). Contrary to what happens in the lung, none of the autophagy messengers RNA tested were regulated by the LMs

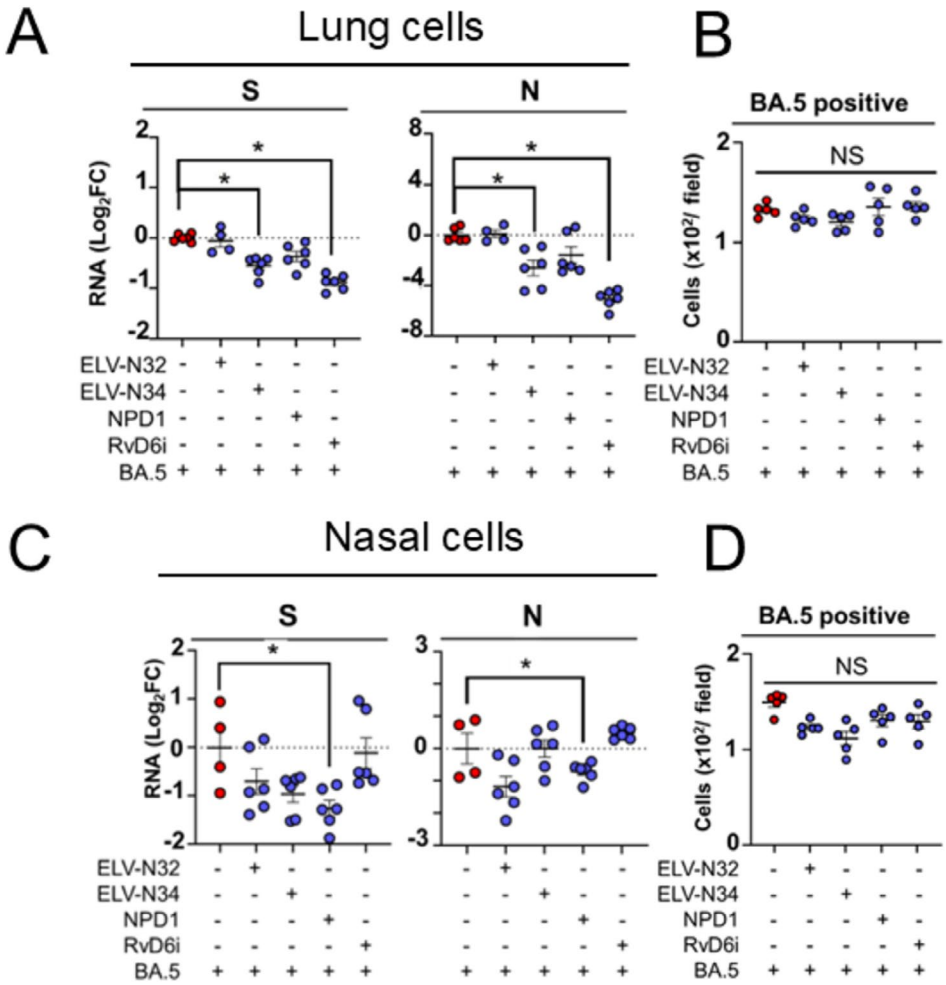

FIGURE 3 | ELV-N34, RvD6i decreased the replication of the virus in lung cells and NPD1 in nasal cells. (A, C) RT-PCR of genomic and subgenomic N and Spike RNAs in lung and nasal cells, respectively, using the experimental design in Figures 1 and 2. (B, D) Number of lung (B) and Nasal (D) cells infected. Infected cells were counted based on the N signal display using Imaris 10.0 cell module. Five replicated samples were analyzed in each case. ANOVA and Tukey's honest significant difference test of the mean were used to determine statistical significance. $^*p < 0.05$.

(data not shown). The diversity of activities of the LMs points to different receptors that may elicit differential efficiencies in counteracting the viral infection.

3.3 | Specific Lipids Decrease the Replication of the Virus in Lung and Nasal Cells

The involvement of the LC3B protein in the SARS-CoV-2 cycle has been proposed to be related to viral replication [25–29]. To determine whether the LMs can reduce viral replication, we quantified Spike and N protein messenger RNA in lung and nasal cells treated for 90 h with ELV-N32, ELV-N34, NPD1, RvD6i, or vehicle following the protocol depicted in Figures 1A and 2A. In lung cells, ELV-N34 and RvD6i reduce the expression of N and S viral RNA (Figure 3A) by 76.7% and 96.9%, respectively. In addition, the N protein is reduced with a consequent decrease in vesicle formation (Figure 1C) by NPD1 as well as ELV-N34 and RvD6i. This suggests that NPD1 may be acting via a different pathway that did not affect the pool of N viral genomic RNA but influenced the sub-genomic counterpart that is translated to be utilized in the folding of the genome, and thus present in vesicular form (Figure 4). In nasal cultures, only NPD1 significantly decreases the expression of N messenger to 61.7%. The overall amount of cells infected (showing N-protein positive signal) did not differ from treatment to vehicle, suggesting that the bioactive lipids halt the replication after the viral entry into the cells. Altogether, these results show that the activity of the LMs reduces intracellular viral replication, is cell type-specific, and does not depend on the strain of the SARS-CoV-2.

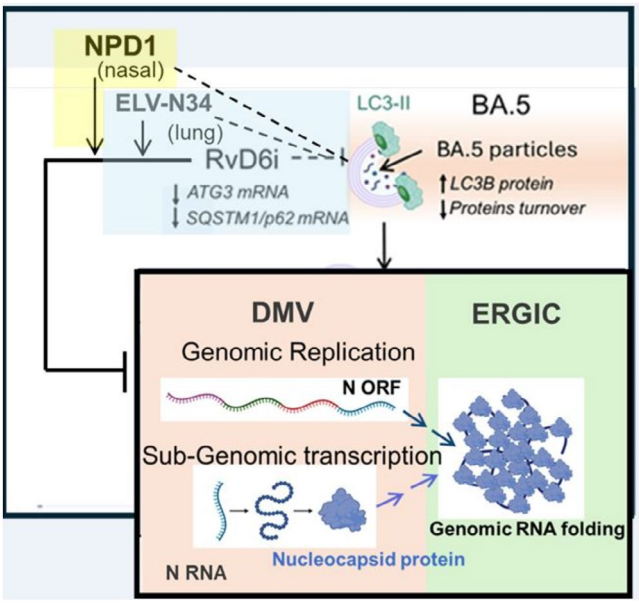

FIGURE 4 | Proposed activity of bioactive lipids during SARS-CoV-2 infection. N protein is required for the folding and packaging of the genomic viral particles in the double-membrane vesicle (DMV). For this purpose, N RNA must be translated into protein (sub-genomic replication of N RNA) to be involved in the packaging of the replication viral genome that contains N RNA. In this manner, the three states of N protein are present in the ERGIC structure (genomic, sub-genomic, and protein), which is the transition between ER and Golgi. Omicron BA.5 increases the formation of vesicles containing N protein in lung and nasal cells. Treatment of lung cells with ELV-N34 and RvD6i, and nasal cells with NPD1 significantly decreases the formation of N-containing vesicles, suggesting the DMV structure is reduced by the LMs.

4 | Discussion

Our study shows that in lung cells, treatment with ELV-N34 and RvD6i decreases N and S messengers (Figure 3A). The corresponding protein signal observed by immunohistochemistry was also decreased in this type of cell infected with two viral strains: the Wuhan and Omicron BA.5 strains. The N RNA messenger and protein are required for the assembly of the viral genome and occur in a structure called ERGIC, formed in the interface of the Golgi and the ER [29, 30] (Figure 4). The formation of this structure is the product of the redirected autophagic host's machinery.

The single-strand virus contains a number of open reading frames (ORF) proteins that are involved in viral replication [10]. One of these proteins is ORF7a, which interfered with the autophagy-lysosome pathway in the endoplasmic reticulum (ER) via interaction with p62 [23, 31–33] and can also start autophagy via the AKT–MTOR-ULK1 pathway. However, the process is limited by activating caspase 3, which cleaves synaptosome-associated protein 29 (SNAP29), leading to an accumulation of the LC3B lipidation complex [31]. In lung cells, we observed an increase in the LC3B protein signal, which forms part of the LC3II lipidation complex. The increase in the LC3B signal is reduced to control levels by the addition of all the LMs tested. In contrast, in nasal cells, elevation of the LC3B was not observed, probably due to the slow dynamic of the viral cycle evidenced by the linear growth with a minor slope without the decay phase when impedance was measured (Figure S5; Table S3).

In other coronaviruses like murine hepatitis virus (MHV) and SARS-CoV, the viral replicase proteins, as well as non-structural proteins, colocalize with the autophagosome marker LC3B [27, 29]. Especially in MHV-infected cells, N protein colocalizes with LC3, this host protein being essential for viral replication, regardless of its lipidation state [27]. We found that a portion of the vesicles containing viral N protein also depicted LC3B in both lung and nasal cells. The number of vesicles with both N and LC3B was increased by the infection of Omicron BA.5, and the lipid mediators reduced the content of these vesicles in all cases, following the pattern of the viral protein content (Figures 1C and 2C). Moreover, evidence shows that LC3 and p62 proteins accumulate in lung samples of COVID-19 patients as a consequence of the viral perturbation of the host's autophagy process [7]. Here, we showed that human lung cells infected with Omicron BA.5 and treated with RvD6i exhibit downregulation of the expression of SQSTM1 mRNA that codes for p62. Recent reports demonstrate that coronaviruses use the protein p62 along with LC3B to transform the host ER into the DMV utilizing their ORF8 protein [30]. By decreasing the availability of p62 messenger and thus its protein, RvD6i may decrease the replication of the virus, as shown in Figure 3A. In addition, RvD6i upregulates the gene expression of C9orf72 [17] and the protein encoded by this gene activates mTORC1 [33]. mTORC1 phosphorylates the transcription factor EB (TFEB on Ser211, causing its inhibition [34]). In BA.5 infected lung cells, RvD6i

also induces downregulation of SQSTM1/p62 and ATG3, two target genes of the TFEB transcription factor consistent with the increase of C9orf72 and consequent activation of mTORC1. Moreover, rapamycin, a potent inhibitor of mTORC1, enhances SARS-CoV-2 entry and replication in animal models by downmodulating intrinsic immunity via disinhibition of TFEB and activation of autophagy [35] by exploiting partially the host's process to fulfill the viral cycle.

In conclusion, treatment of SARS-CoV-2–infected human lung and nasal cells with bioactive lipids derived from DHA shows inhibition of viral autophagy process and, as a consequence viral replication. These novel findings of LMs acting as antiviral can be potentially a complement treatment to vaccination.

Author Contributions

N.G.B., J.M.C., and H.E.P.B. designed the experiments and wrote the manuscript. N.J.M. ran the xCELLigence RTCA eSight – Imaging and Impedance – Agilent and infected the cells, and M.-A.I.K. performed Biomark real-time PCR. S.B. cultured the lung and nasal cells, and J.M.C. did the immunocytochemistry and analyzed all the data.

Acknowledgments

This work was supported by the EENT Foundation of New Orleans.

Conflicts of Interest

The authors declare no conflicts of interest.

Data Availability Statement

Data available upon request from the authors.

References

1. P. V. Markov, M. Ghafari, M. Beer, et al., "The Evolution of SARS-CoV-2," *Nature Reviews Microbiology* 21 (2023): 361–379.

2. S. Farheen, Y. Araf, Y.-D. Tang, and C. Zheng, "The Deltacron Conundrum: Its Origen and Potential Health Risks," *Journal of Medical Virology* 94 (2022): 5096.

3. G. Li, R. Hilgenfeld, R. Whitley, and E. De Clercq, "Therapeutic Strategies for COVID-19: Progress and Lessons Learned," *Nature Reviews Drug Discovery* 22 (2023): 449–475.

4. C. Chakraborty, M. Bhattacharya, A. Alshmmari, M. Alharbi, and C. Zheng, "Exploring the Structure and Molecular Interacion Landscape of Nirmatrevil and Mpro Complex: The Study Might Assist in Designing More Potent Antivirals Targeting SARS-CoV-2 and Other Virus," *Journal of Infection and Public Health* 16 (2023): 1961–1970.

5. L. Koepke, M. Hirschenberger, M. Hayn, F. Kirchoff, and K. M. Saprrer, "Manipulation of Autophagy by SARS-CoV-2 Proteins," *Autophagy* 17, no. 9 (2021): 259–2661.

6. W. I. Twu, J. Y. Lee, H. Kim, et al., "Contribution of Autophagy Machinary Factors to HCV and SARS-CoV-2 Replication Organelle Formation," *Cell Reports* 37 (2021): 110049.

7. N. C. Gassen, J. Papies, T. Bajaj, et al., "SARS-CoV-2-Mediated Dysregulation of Metabolism and Autophagy Uncovers Host-Targeting Antivirals," *Nature Communications* 12 (2021): 3818.

8. S. Guo, X. Lei, Y. Chang, et al., "SARS-CoV-2 Hijacks Cellular Kinase CDK2 to Promote Viral RNA Synthesis," *Signal Transduction and Targeted Therapy* 7 (2022): 400.

9. F. S. Mesquita, L. Abrami, L. Bracq, et al., "SARS-CoV-2 Hijacks a Cell Damage Response, Which Induces Transcription of a More Efficient Spike S-Acyltransferase," *Nature Communications* 14 (2023): 7302.

10. P. Roingeard, S. Eymieux, J. Burlaud-Gaillard, C. Hourioux, R. Patient, and E. Blanchard, "The Double-Membrane Vesicle (DMV): A Virus-Induced Organelle Dedicated to the Replication of SARS-CoV-2 and Other Positive-Sense Single-Stranded RNA Viruses," *Cellular and Molecular Life Sciences* 79 (2022): 425.

11. S. Bhattacharjee, B. Jun, L. Belayev, et al., "Elovanoids Are a Novel Class of Homeostatic Lipid Mediators That Protect Neural Cell Integrity Upon Injury," *Science Advances* 3 (2017): e1700735.

12. N. G. Bazan, "Docosanoids and Elovanoids From Omega-3 Fatty Acids Are Pro-Homeostatic Modulators of Inflammatory Responses, Cell Damage and Neuroprotection," *Molecular Aspects of Medicine* 64 (2018): 18–33.

13. J. M. Calandria, S. Bhattacharjee, N. J. Maness, et al., "Elovanoids Downregulate SARS-CoV-2 Cell-Entry, Canonical Mediators and Enhance Protective Signaling in Human Alveolar Cells," *Scientific Reports* 11 (2021): 12324.

14. A. Resano, S. Bhattacharjee, M. Barajas, et al., "Elovanoids Counteract Inflammatory Signaling, Autophagy, Endoplasmic Reticulum Stress, and Senescence Gene Programming in Human Nasal Epithelial Cells Exposed to Allergens," *Pharmaceutics* 14 (2022): 113.

15. K. V. Do, M. A. I. Kautzmann, B. Jun, et al., "Elovanoids Counteratac Oligomeric β-Amyloid-Induced Gene Expression and Protect Photoreceptors," *Proceedings of the National Academy of Sciences of the United States of America* 116 (2019): 24317–24325.

16. T. L. Pham, A. H. Kakazu, J. He, B. Jun, N. G. Bazan, and H. E. P. Bazan, "Novel RvD6 Stereoisomer Induces Corneal Nerve Regeneration and Wound Healing Post-Injury by Modulating Trigeminal Transcriptomic Signature," *Scientific Reports* 10 (2020): 4582.

17. T. L. Pham, A. H. Kakazu, J. He, et al., "Elucidating the Structure and Functions of Resolvin D6 Isomers on Nerve Regeneration With a Distinctive Trigeminal Transcriptome," *FASEB Journal* 35, no. 8 (2021): e21775, https://doi.org/10.1096/fj.202100686R.

18. T. L. Pham, J. He, A. H. Kakazu, et al., "ELV-N32 and RvD6 Isomer Decrease Pro-Inflammatory Cytokines, Senescence Programming, ACE2 and SARS-CoV-2-Spike Protein RBD Binding in Injured Cornea," *Scientific Reports* 11 (2021): 12787.

19. T. Takahashi, M. K. Ellingson, P. Wong, et al., "Sex Differences in Immune Response That Underline COVID-19 Disease Outcomes," *Nature* 588 (2020): 315.

20. N. Amruta, N. J. Maness, T. E. Gressett, Y. Tsuchiya, M. Kishi, and G. Bix, "Effect of Acetic Acid Inactivation of SARS-CoV-2," *PLoS One* 18 (2023): e0276578.

21. M. M. Reid, L. Belayev, L. Khoutorova, et al., "Integrated Inflammatory Signaling Landscape Response After Delivering Elovanoid Free-Fatty-Acid Precursors Leading to Experimental Stroke Neuroprotection," *Scientific Reports* 13 (2023): 15841.

22. S. Li, X. Li, H. Liang, et al., "SARS-CoV-2 ORF7a Blocked Autophagy Flux by Intervening in the Fusion Between Autophagosome and Ltsosome to Promote Viral Infection and Pathogenesis," *Journal of Medical Virology* 95 (2023): e29200.

23. S. Ghosh, T. A. Dellibovi-Ragheb, A. Kerviel, et al., "β-Coronaviruses Use Lysosomes for Egress Instead of the Biosynthetic Secretory Pathway," *Cell* 183 (2020): 1520–1535.e14.

24. R. C. M. C. Silva, J. S. Ribeiro, G. P. D. da Silva, L. J. da Costa, and L. H. Travassos, "Autophagy Modulators in Coronavirus Diseases: A Double Strike in Viral Burden and Inflammation," *Frontiers in Cellular and Infection Microbiology* 12 (2022): 845368.

25. P. V'kovski, A. Kratzel, S. Steiner, H. Stalder, and V. Thiel, "Coronavirus Biology and Replication: Implications for SARS-CoV-2," *Nature Reviews Microbiology* 19, no. 3 (2021): 155–170, https://doi.org/10.1038/s41579-020-00468-6.

26. G. Wolff, R. W. A. L. Limpens, J. C. Zevenhoven-Dobbe, et al., "A Molecular Pore Spans the Double Membrane of the Coronavirus Replication Organelle," *Science* 369 (2020): 1395–1398.

27. E. Prentice, W. G. Jerome, T. Yoshimori, N. Mizushima, and M. R. Denison, "Coronavirus Replication Complex Formation Utilizes Components of Cellular Autophagy," *Journal of Biological Chemistry* 279 (2004): 10136–10141.

28. A. Shroff and T. Y. Nazarko, "The Molecular Interplay Between Human Coronavirus and Autophagy," *Cells* 10 (2021): 2022.

29. F. Reggiori, I. Monastyrska, M. H. Verheije, et al., "Coronaviruses Hijack the LC3-I-Positive EDEMosomes, ER-Derived Vesicles Exporting Short-Lived ERAD Regulators, for Replication," *Cell Host & Microbe* 7 (2010): 500–508.

30. X. Tan, K. Cai, J. Li, et al., "Coronavirus Subverts ER-Phagy by Hijacking FAM134B and ATL3 Into p62 Condensates to Facilitate Viral Replication," *Cell Reports* 42 (2023): 112286.

31. P. Hou, X. Wang, H. Wang, et al., "The ORF7a Protein of SARS-CoV-2 Initiates Autophagy and Limits Autophagosome-Lysosome Fusion via Degradation of SNAP29 to Promote Virus Replication," *Autophagy* 19 (2023): 551–569.

32. Y. Han, H. Zhou, C. Liu, W. Wang, Y. Qin, and M. Chen, "SARS-CoV-2 N Protein Coordinates Viral Particle Assembly Through Multiple Domains," *Journal of Virology* 98 (2024): e0103624.

33. J. Smeyers, E.-G. Banchi, and M. Latouche, "C9ORF72: What It Is, What It Does, and Why It Matters," *Frontiers in Cellular Neuroscience* 15 (2021): 661447.

34. A. Roczniak-Ferguson, C. S. Petit, F. Froehlich, et al., "The Transcription Factor TFEB Links mTORC1 Signaling to Transcriptional Control of Lysosome Homeostasis," *Science Signaling* 5, no. 228 (2012): ra42, https://doi.org/10.1126/scisignal.2002790.

35. G. Shi, A. I. Chiramel, T. Li, et al., "Rapalogs Downmodulate Intrinsic Immunity and Promote Cell Entry of SARS-CoV-2," *Journal of Clinical Investigation* 132, no. 24 (2022): e160766, https://doi.org/10.1172/JCI160766.

Supporting Information

Additional supporting information can be found online in the Supporting Information section.